

Stress response function of a granular layer: Quantitative comparison between experiments and isotropic elasticity

D. Serero¹, G. Reydellet¹, P. Claudin^{1,a}, É. Clément¹, and D. Levine²

¹ Laboratoire des Milieux Désordonnés et Hétérogènes (UMR 7603 du CNRS), 4 place Jussieu, case 86, 75252 Paris Cedex 05, France

² Technion-Israel Institute of Technology, Physics Department, 32000 Haifa, Israel

Received 3 August 2001

Abstract. We measured the vertical pressure response function of a layer of sand submitted to a localized normal force at its surface. We found that this response profile depends on the way the layer has been prepared: all profiles show a single centered peak whose width scales with the thickness of the layer, but a dense packing gives a wider peak than a loose one. We calculate the prediction of isotropic elastic theory in the presence of a bottom boundary and compare it to the data. We found that the theory gives the right scaling and the correct qualitative shape, but fails to really fit the data.

PACS. 46.25.-y Static elasticity – 45.70.Cc Static sandpiles; granular compaction – 83.80.Fg Granular solids

1 Introduction

The statics of granular materials has been receiving recently a lot of attention, for a review see *e.g.*, [1]. An important issue is still to understand the mechanical status of an assembly of non-cohesive grains. In the small deformation limit, a classical viewpoint assumes a behavior akin to an effective elastic medium. At a given confinement pressure, linear relations between stress and strain are measured and for larger strains, another picture is proposed based on a plastic modelling of the stress-strain relations. Therefore, for all practical purposes the available models used to describe granular matter in the quasi-static limit are of the elasto-plastic class with constitutive parameters determined empirically from standard triaxial tests [2]. This elastic viewpoint is somehow corroborated by ultrasound propagation experiments where, under large confining pressure, elastic moduli of p and s waves produced by a localized pulse can be measured [3]. However, sound propagation measurements also evidence a strong “speckle-like” component associated with the intricate contact force paths topology or “force chains” network. In a granular packing, contact forces of amplitude larger than the average were found to organize in cells of sizes of about 10 grains diameters [4]. The fragile character of these structures is even more obvious at low confining pressure where, for example, ultra-small perturbations within the pile can completely modify the sound response spectrum [5]. More generally, subtle self-

organization properties of the contact force network (also called the texture) were evidenced by thorough numerical studies by Radjai *et al.* [4].

At a macroscopic level, the pressure profile under the base of a sand heap built from a point source (*i.e.* from a hopper outlet), shows a minimum below the apex, but *does not* when the heap is constructed by successive horizontal layers [6,7]. This surprising effect is currently viewed as a signature of the preparation history. Successive avalanches originated from the hopper outlet could have embedded a microscopic structure which is reflected macroscopically by an arching effect below the apex.

The ability for a granular piling to change its texture (granular contact network, force chains geometry) in response to an external constraint, have cast legitimate suspicions on the fundamental validity of elasticity for packing of hard grains. For these reasons, a new class of models—called OSL for “Oriented Stress Linearity”—was introduced by Bouchaud *et al.* [8], which could explain remarkably well the sandpile data [9], as well as stress screening in silos [10]. These models have been the subject of a rather controversial debate [11]. One of the reasons for that was the fact that they do not belong to the standard elasto-plastic class. As a matter of fact, they do not require the introduction of a displacement field, and the usual stress-strain relations are rather replaced by “stress-only” ones which encode the history-dependent state of equilibrium of the piling. In particular, the equations governing the stress distribution in these models are of hyperbolic type, which contrasts with the elliptic (or mixed elliptico-hyperbolic)

^a e-mail: claudin@ccr.jussieu.fr

equations of elastic (or elasto-plastic) modellings. An attractive feature of hyperbolic equations is that they have characteristic lines along which stress is transmitted, and which were argued to be the mathematical transcription of force chains that one can clearly see in granular systems [12].

Measurements of the pressure response of a layer of sand submitted to a localized normal force at its surface soon appeared to be a way to discriminate between the different classes of models [1]. Such a crucial experiment addresses at the deepest level questions on the real mechanical status for a granular assembly. In elasticity, the shape of this pressure profile shows a single centered broad peak, whose width scales with the height h of the layer [13]. On the contrary, OSL models predict a response with two peaks (or a ring in three dimensions) on each side of the overloaded point. Experiments [14–16] and simulations [17, 18] have then been performed recently. Although the picture is far from being completely clear yet, the conclusions of these works can be roughly summarized as follows. For disordered systems, experiments definitively show elastic-like response, while regular packing exhibits OSL features. A third class of granular assemblies have also macroscopic equilibrium equations of the hyperbolic type: packings that can be prepared under the special isostaticity condition [19, 20], defining the uniqueness of the contact forces once the list of contacts is known [21, 22]. In practice, this condition would correspond to a minimum number of contact per grains, such as frictionless contact forces for $2d$ random packing. A recent numerical result obtained for such an assembly explicitly shows an OSL-like propagation as a response to a localized force (at least on a scale up to 20 grains size) [23]. Note at last that, by contrast, the experiment presented in [24] rather claims a “diffusive” response function, in agreement with the stochastic scalar q -model [25] but these experiments were performed on a small size packing and in a rather specific geometry.

In this paper, we present response function measurements obtained on large pilings made of natural sand. We show that it is possible to get rather different pressure profiles when preparing the packing with two different procedures. As in [14], we found that elastic predictions give the right scaling and the correct qualitative shape but, here, we perform a quantitative comparison between experimental data and isotropic elasticity predictions. We seek to answer precisely the question whether stress transmission properties can still be described using an isotropic elastic medium theory. What we found is that elasticity actually fails to really fit the data.

The paper is organized as follows. In Section 2 we expose how the measures are done and the way the data are calibrated. Then we show how different data sets can be obtained, depending on the sample preparation method. Section 3 is devoted to the calculation of the stress components at the bottom of an isotropic elastic layer of finite thickness h . In order to make this paper easier to read, the details of these calculations are given in appendices A and B for the two- and three-dimensional cases, respectively.

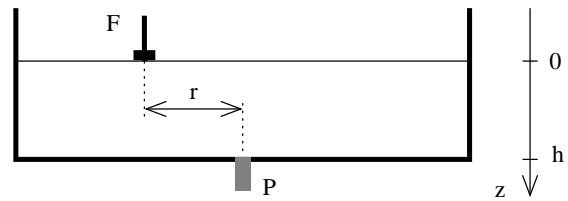


Fig. 1. Sketch of the experimental set-up. A localized vertical force F is applied on the top surface of the granular layer ($z = 0$). The corresponding pressure response on the bottom is measured at some distance r from that point. The vertical z -axis points downwards and we note h the thickness of the layer (between 0 and 10 cm). We use natural “Fontainebleau” sand whose typical diameter is ~ 0.3 mm.

The comparison between the experiments and elasticity is done in Section 4. At last, we conclude the paper with a discussion on the interpretation of the results in Section 5.

2 The response function experiment

The experimental technique that we use for the measure of the pressure response of a granular layer to the application of a localized vertical force F at its top surface has been described in detail in [14]. The sketch of the set-up can be seen in Figure 1. Briefly, the pressure P is measured by the tiny change of the electrical capacity of the probe due to the slight deformation of its top membrane. F is applied with a piston whose displacement is monitored and controlled to stay as small as possible (less than $500 \mu\text{m}$). To gain sensitivity, F is modulated at a frequency f , and the probe signal is directed to a lock-in amplifier synchronized at f too. Any choice of f between 0.1 and 80 Hz gives the same result. We checked that the response P is linear in F . Both piston and probe have a surface in contact with the grains of $\sim 1 \text{ cm}^2$. The container is large enough ($50 \times 50 \text{ cm}^2$) to be able to neglect finite-size effects due to the lateral walls. Its bottom plate is very rigid (Duraluminium, thickness 2 cm), and covered by a sheet of sand paper, in order to avoid sliding of the grains on the plate.

We call r the horizontal distance between the piston and the probe. In order to measure the profile $P(r)$, it is easier to vary r by moving the piston. In principle, the horizontal integral of the pressure profiles $F^* = \int_0^{+\infty} dr 2\pi r P(r)$ should be constant and equal to the force F applied at the surface. In fact, due to arching screening effects around the probe, this integral actually shows a large dispersion — see Figure 2 — from an experiment to another and remains less than F . We estimate the ratio F^*/F to be of order 80%. It is difficult to say if there is a systematic variation of F^* as a function of the layer thickness h or not — taking such a dependency into account would lead to non-linear effects such as those evoked in [26] that we neglected for simplicity. This screening effect is well known to be inherent to every measurement of stresses in granular materials [11], but we could get rid of this problem of screening by using F^* to renormalize

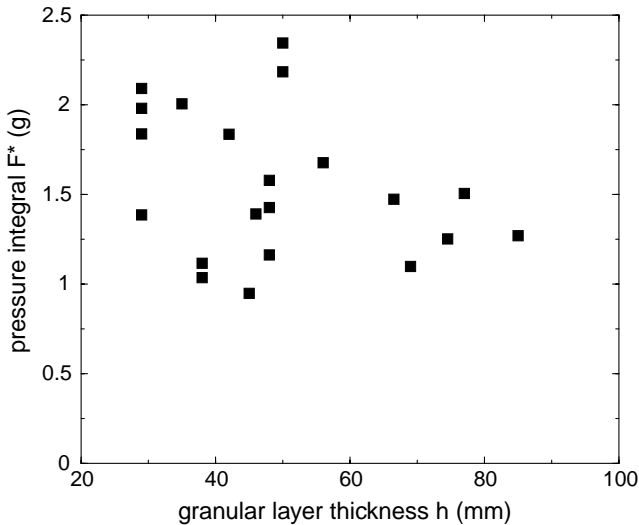


Fig. 2. This plot shows the integral F^* of the profiles $P(r)$ taken from different experiments.

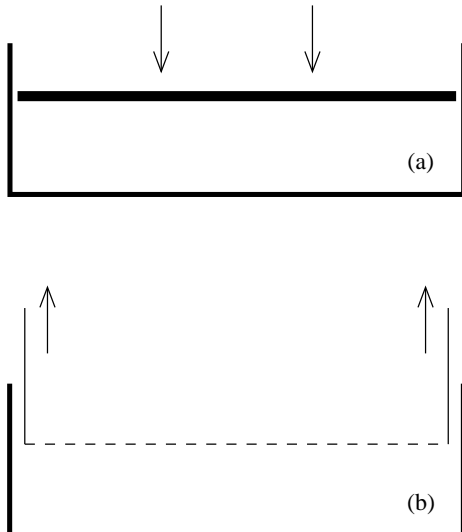


Fig. 3. The packing of the grains has been prepared in two different ways: we either make it very dense (compacity ~ 0.7) by pushing hard on the grains with a metallic plate (a), or very loose (compacity ~ 0.6) by pulling up a sieve through them (b).

the pressure measurements: $P \leftarrow \frac{1}{F^*}P$. The accurate determination of F^* is a crucial point when it comes to the quantitative comparison between experiments and theory. In particular, we were very careful to take enough data points to have a good estimation of the experimental offset at large r .

A particular attention should be paid to the way the granular layer has been prepared. In order to observe different mechanical behavior, we chose two extreme procedures. They are schematized in Figure 3. The first one consists in making a packing as dense as possible. We add the sand by layers of 0.5 cm and after each layer, we push hard on the grains with a metallic plate. We can then

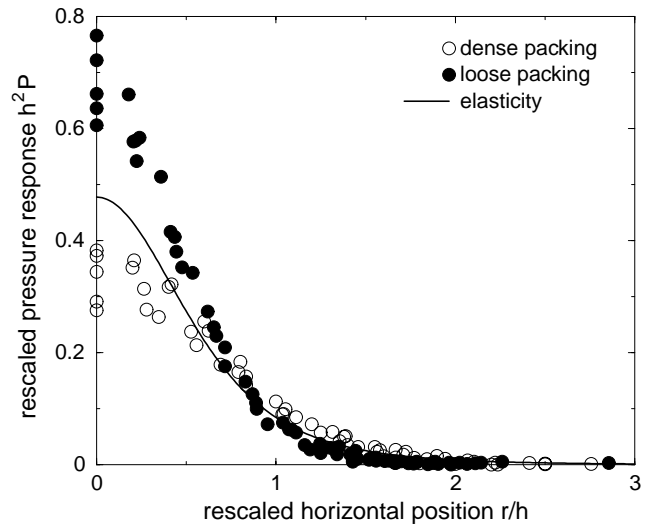


Fig. 4. The pressure response profile depends on the way the system of grains was prepared: it is broader for a dense packing (empty circles) than for a loose one (filled circles). The response of a semi-infinite isotropic elastic medium (solid line) lays in between. For a given preparation, the experimental data collapse pretty well when renormalized by their F^* factor —see text— and rescaled by the height h of the layer. Here, we have plotted together measures on layers whose thickness varies from $h \sim 30$ to $h \sim 60$ mm.

reach a compacity of order of 0.7 —note that this “layer by layer” procedure may create inhomogeneities in the density field. By contrast, to make the packing very loose, we first place a sieve on the bottom plate of the container, pour the grains into the box, and then gently pull up the sieve all through the grains. The corresponding compacity is of order of 0.6.

As already mentioned in [14], data taken from layers of several heights can be plotted together by rescaling lengths by h —which contradicts the “diffusive” description as proposed by the q -model. The rescaled data h^2P as a function of r/h can be seen in Figure 4. This plot clearly shows that the response of the granular layer is “history dependent”: the pressure profile of a dense packing is much broader than that of a loose one.

Bousinesq and Cerruti gave the expression of the stress response in the case of a isotropic semi-infinite elastic medium submitted to a localized and vertical unitary force F at $r = 0$ [27]. For the vertical pressure at point (r, z) , this expression is

$$\sigma_{zz} = \frac{3F}{2\pi} \frac{z^3}{(r^2 + z^2)^{5/2}}. \quad (1)$$

This formula is independent of the Poisson coefficient ν of the elastic material and thus does not have any adjustable parameter. It is therefore unable to reproduce the two different experimental pressure profiles. As a matter of fact, this function lays in between the two profiles —see Figure 4. The pressure responses of a dense and a loose packing of sand are thus, respectively, broader and narrower than the standard elastic response profile.

In the next section, we shall take into account the finite thickness of the layer and derive the corresponding expressions for the stresses, which will indeed depend on ν . These expressions will then be quantitatively compared to the experimental data.

3 Elastic calculations

In this section, we derive the expressions of the stress tensor components at the bottom of an isotropic elastic layer of finite thickness h . This calculation is not new, but as far as we know, the available literature only provides numerical tables [28] that make fits difficult to perform. Such a calculation is a bit heavy, and we chose to present here its main lines only. The full details can be found in appendices A and B for the two- and three-dimensional cases, respectively. The formalism we use and the way the calculation is led is directly inspired from [13, 29].

The stress state of an elastic material is described by its stress tensor components σ_{ij} . At equilibrium, these quantities must verify the force balance equations:

$$\nabla_i \sigma_{ij} = \rho g_j, \quad (2)$$

where ρ is the density of the material and g_j the gravity vector. These relations are not enough to form a closed system of equations. An additional physical input is required. In plain elasticity theory, a displacement field u_i is introduced—it measures the change in position, with respect to the reference state where no constraints are applied—and the corresponding strain tensor $u_{ij} = \frac{1}{2} \left(\frac{\partial u_i}{\partial x_j} + \frac{\partial u_j}{\partial x_i} \right)$ is related to the stresses via linear relations which involve two parameters which characterize this pure elastic material: its Young modulus Y and its Poisson coefficient ν .

It is possible to express all the equations in terms of the stress components only. Eliminating the u_{ij} , one gets

$$(1 + \nu) \Delta \sigma_{ij} + [1 + (3 - d)\nu] \frac{\partial^2 \sigma_{kk}}{\partial x_i \partial x_j} = 0, \quad (3)$$

where d is the space dimension—these equations are not valid in the case of a non-uniform external body force. In particular, contracting i and j , we see that the trace of the stress tensor is a harmonic function, *i.e.* that $\Delta \sigma_{kk} = 0$. These relations include (derivatives of) the force balance equations (2). Taking the Laplacian of (3), we also see that the σ_{ij} are bi-harmonic.

The solutions of equations (3) can be found in Fourier transforms. Let first focus on the two-dimensional (x, z) case. Because $\Delta \Delta \sigma_{ij} = 0$, the general form of the vertical pressure σ_{zz} can be written as follows:

$$\sigma_{zz} = \int_0^{+\infty} dq \cos(qx) \left\{ [A_{zz}^+(q) + qz B_{zz}^+(q)] e^{qz} + [A_{zz}^-(q) + qz B_{zz}^-(q)] e^{-qz} \right\}. \quad (4)$$

The expression for σ_{xx} is very similar. For the shear stress σ_{xz} , the cosine factor should be replaced by $\sin(qx)$. In

fact, only four of these twelve functions A 's and B 's are independent. They are fully determined by the boundary conditions, and we can get this way explicit—but integral—expressions for the stresses.

In elliptic problems like elasticity, stress or strain conditions must be specified on *all* the boundaries. Our aim here is to calculate the response of a layer of height h submitted to a localized pressure at its top surface. We then suppose that the “piston” which applies this overload is perfectly smooth and imposes, for example, a normalized ($F = 1$) Gaussian profile $Q(x)$ for the vertical pressure

$$Q(x) = \frac{1}{\sqrt{2\pi\sigma^2}} e^{-x^2/2\sigma^2}, \quad (5)$$

where σ is the adjustable width of this overload. The two conditions at the top are then i) $\sigma_{zz}(x, 0) = Q(x)$ and ii) $\sigma_{xz}(x, 0) = 0$. Concerning the bottom, we assume that it is perfectly rigid, such that iii) $u_z(x, h) = 0$, and either very smooth or very rough. The last boundary condition is then iv-a) $\sigma_{xz}(x, h) = 0$ or iv-b) $u_x(x, h) = 0$, respectively.

Integrations in both smooth and rough bottom cases can be done numerically, and the corresponding results for the stress response σ_{ij} are plotted in Figure 5. These integrations have been done for the specific choice of a very peaked Gaussian overload: $\sigma = 0.001h$ —a quasi- δ -function. For comparison, these plots are shown together with the Green's function of a vertically semi-infinite medium.

All three σ_{zz} curves have roughly the same shape. This is no longer true when we plot the horizontal pressure instead of the vertical one: σ_{xx} is proportional to σ_{zz} (see Eq. (A.15)) for a rough bottom, but shows a double peak for a semi-infinite medium as well as for a smooth bottom—with a large negative central part. Negative values can be also seen for σ_{zz} in Figure 5, especially for the case of a smooth bottom. They are absolutely admissible for elastic material—no delamination between the material and the bottom is allowed.

An interesting and rather non-intuitive point is that the finiteness of the elastic layer narrows the stress response. Only the response on the rough bottom depends on the value of the Poisson coefficient. We chose $\nu = 0.3$. This dependence is very weak for σ_{zz} —see inset of Figure 5. At last, it should be noted that all these curves scale with the height h .

The axi-symmetric three-dimensional calculation is very similar, except that trigonometric functions have to be replaced by Bessel ones in equations like (4). Again, a numerical integration of the functions A 's and B 's can be done for a Gaussian overload, and the corresponding pressure profiles in both smooth and rough cases are plotted in Figure 6. They are also compared to the semi-infinite solution. The $3d$ results are qualitatively the same as in two dimensions. The wideness of the response function is non-monotonic with the Poisson ratio and presents a maximum for $\nu \sim 0.27$. A slight difference is that not only the $3d$ solution for the rough bottom depends on the Poisson coefficient, but the smooth bottom solution too. Again, this dependence is very weak for the vertical component of the stress tensor.

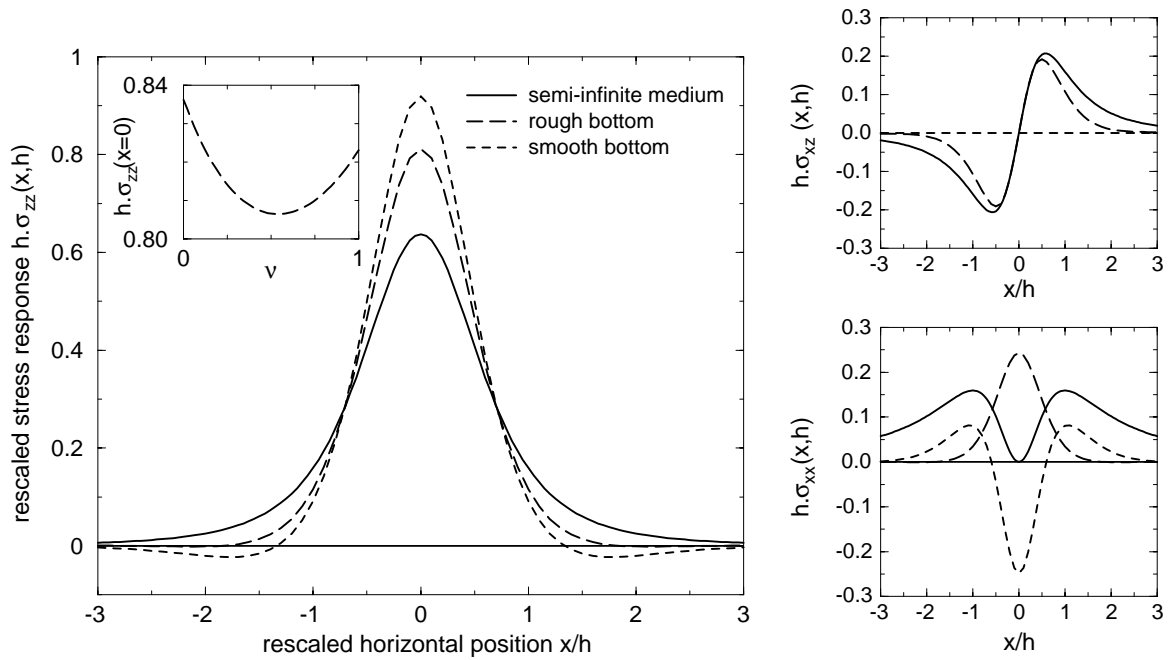


Fig. 5. Stress response functions for a two-dimensional elastic material. The main plot compares the pressure profile of a semi-infinite system at depth $z = h$, with the response of a finite elastic layer of thickness h with either a rough or a smooth bottom. The first and third curves of each plot are independent of the Poisson coefficient ν . For the second one, we chose $\nu = 0.3$ but its shape depends only very weakly on the value of ν —see inset where the maximum of the response has been plotted against ν . Note that in $2d$ elasticity we must have $\nu \leq 1$. The side plots show the other components of the stress tensor (shear and horizontal pressure).

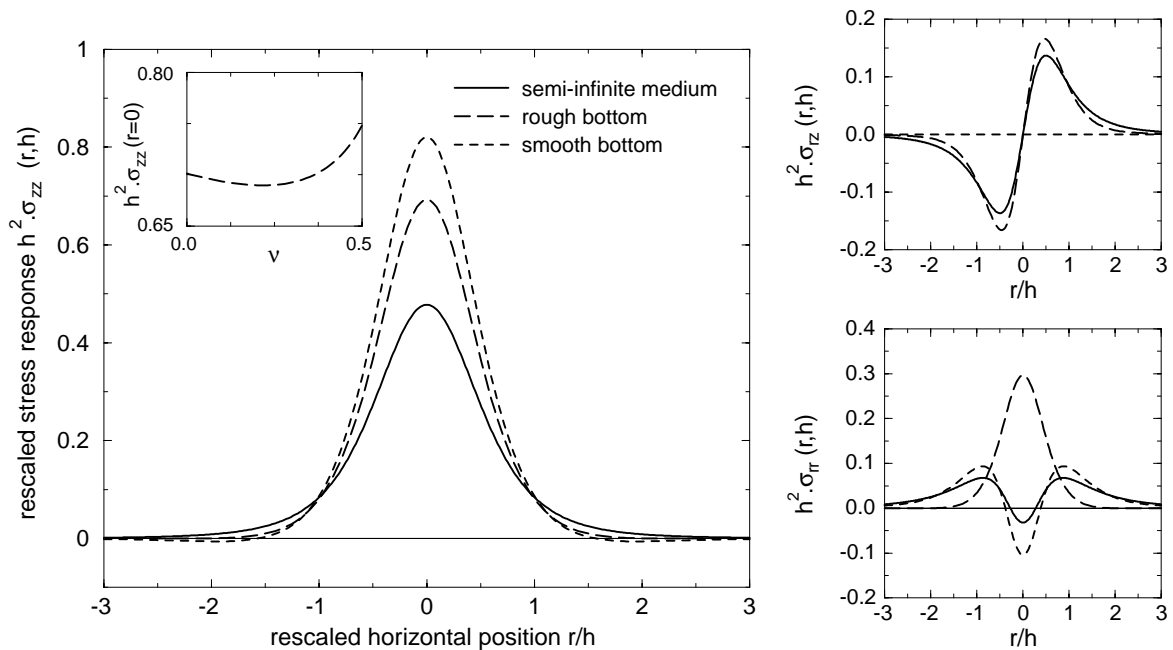


Fig. 6. $3d$ equivalent of Figure 5 —now the largest acceptable value for ν is $1/2$. We chose again $\sigma = 0.001h$ and $\nu = 0.3$. The results are qualitatively the same as in two dimensions.

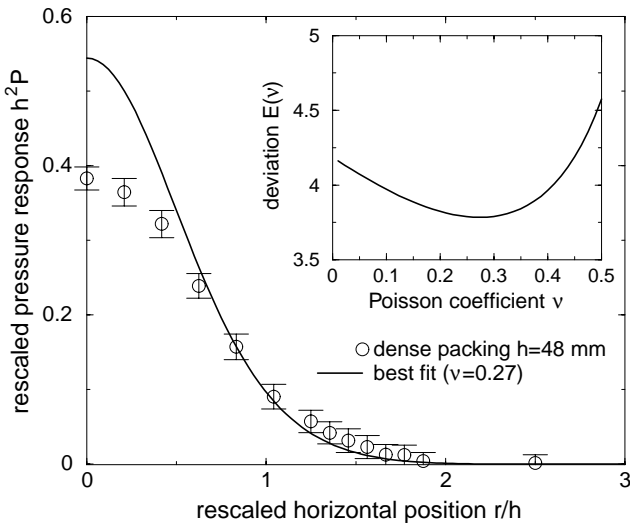


Fig. 7. Fit of the data obtained on a dense packed granular layer. It is rather poor because the elastic response cannot get wide enough. The inset shows the deviation E versus ν . $\nu = 0.27$ corresponds to $E = 3.8$.

4 A quantitative comparison

In this section, we want to compare quantitatively the pressure response measurements with the elastic predictions. Among the two cases calculated in the previous section (rough and smooth bottom), the first one is the closest to our experimental situation —we checked that the shear stress at the bottom of the grain layer is finite. Therefore, only rough bottom elastic formulae are going to be used for the following fits.

A set of experimental data is a file with three columns: the horizontal distance between the piston and the probe r_k , the corresponding pressure measurement P_k and its typical dispersion ΔP_k . There are $N_e \sim 15$ such triplets for one pressure profile. As explained in Section 2, the data have been renormalized by their factor F^* in order to be of integral unity.

We quantify the “distance” between the experimental pressure profile P and the elastic predictions σ_{zz} by computing the average quadratic deviation E :

$$E^2 = \frac{1}{N_e} \sum_{k=1}^{N_e} \left(\frac{P_k - \sigma_{zz}(r_k, h)}{\Delta P_k} \right)^2. \quad (6)$$

$E = 1$ would mean that a typical distance between theory and experimental data is one error bar. A value of E larger than 1 will then be considered as not good. Because σ_{zz} depends on the Poisson coefficient ν , E is also a function of ν . This function has a minimal value which gives the best fitting ν . The precision of this value depends on the sharpness of this minimum.

The results of our fits are gathered together in Figure 9. The results can be summarized as follows. In the case of a dense packing, the experimental response function is too wide to be well fitted by an elastic curve —see Figure 7. As a matter of fact, we get typically $E \sim 4$ for the

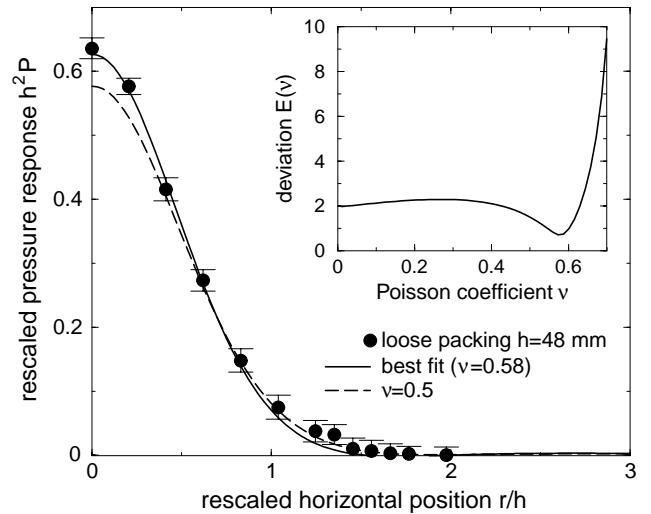


Fig. 8. Fit of the loose packing data. The best Poisson coefficient exceeds the usual $\nu = \frac{1}{2}$ limit. $\nu = 0.58$ corresponds to $E = 0.6$, but $E = 1.5$ when $\nu = 0.50$.

best fit. The corresponding Poisson coefficient value does not then have any real meaning. For the loose packing, the situation is different. The experimental data, though closer to the elastic response, lay on a curve which is too narrow to be properly fitted. The best value of ν is then $\nu = \frac{1}{2}$ which gives the most narrow elastic response, corresponding to $E \sim 2$. Interestingly, however, if one allows ν to exceed the standard bound $\nu = \frac{1}{2}$, one can fit the data pretty well —see Figure 8. This excess can be done mathematically because the qualitative shape of the stress profiles calculated with the elasticity theory changes for $\nu \geq \frac{3}{4}$ only, leading beyond this value to oscillatory behaviours —see the appendices. Note that the dilatancy effect in granular material has sometimes been argued to be somehow encoded by a Poisson coefficient larger than $\frac{1}{2}$, which is the “incompressibility” limit. Although we do not think that dilatancy can be treated with the concepts of reversible elasticity, our results would contradict such an argument because only dense packings dilate, loose ones on the contrary contract.

As we said in Section 2, the piston which applies the overload at the top surface of the layer as well as the pressure probe have an area of $\sim 1 \text{ cm}^2$. Taking into account the finite size of the piston for the fits was easy in our elastic formalism. Indeed, we assumed that the overload had a Gaussian profile of adjustable width σ , which was then simply set to the piston diameter. By contrast, taking into account that of the pressure probe requires the convolution of the elastic formulae with a disk of finite diameter. This calculation is much less easy and makes the computation of the stress profiles difficult to do. In fact, we checked on few data sets that these two finite-size effects are not very important as soon as the layer thickness h is larger than $\sim 30 \text{ mm}$, *i.e.* 3 piston/probe diameters. The actual values of E and ν that come out from these modified fits are a bit different —slightly better— than that

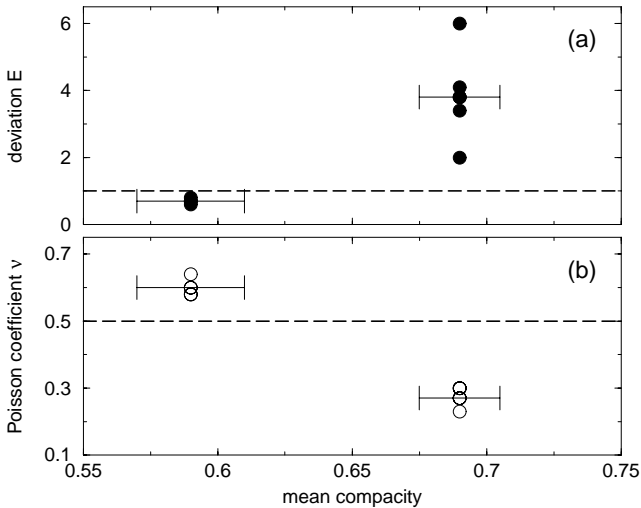


Fig. 9. This figure shows (a) the best elasticity fit quality E and (b) the corresponding value for the best Poisson ratio ν as a function of the compacity of the packing. Above the dash line $E = 1$, the fits are not in good agreement with the data. Only points under the dash line $\nu = \frac{1}{2}$ are in principle valid in the elastic framework.

of Figure 9, but the conclusions written in the previous paragraph stay exactly the same.

5 Discussion and conclusions

As was shown that the stress profile under a sandpile does or does not have a “dip” below the apex of the pile, we found that the pressure response of a layer of sand submitted to a localized normal force at its top surface depends on the way this layer has been built —its “history”. The response is rather wide when the grain packing is made very dense and compact, but it is more narrow when the layer is loose. For a given height, the maximal value of the pressure is approximately twice smaller in the first than in the second case. The predictions of isotropic elasticity theory, even when taking into account the finite layer thickness, agree poorly with the experimental data. However, note the puzzling result that, taking a Poisson coefficient larger than the usual bound $\frac{1}{2}$, can fit rather well the experimental data for the loose packing preparation. We have no interpretation of this fact besides concluding for the non-adequacy of the isotropic elastic picture for piling prepared using “dense” or “loose” filling procedures.

Although we present all our results in terms of dense or loose packing, the compacity in itself is certainly not a good control parameter. Rather, a natural way to improve the fits within this elastic framework would be to take into account a possible anisotropy of the material. A classical example is the so-called “anelotropy” which occurs when the vertical symmetry axis has different mechanical properties than the horizontal directions. Such an anisotropy has five independent parameters: two Poisson coefficients (a vertical and a horizontal one), two Young moduli (*idem*) and a shear modulus. A theory with so many parameters

will for sure fit our data. Indeed, the shear modulus has been found to be of strong influence on the shape of the response function [30].

We think, however, that a standard elastic description of granular materials is unsatisfactory: a proper definition of the kinetic variables may be problematic for systems of hard particles. As a matter of fact, the link between the local microscopic movement of the grains and the possible corresponding large-scale displacement field is a current subject of research [31]. Recent numerical simulations of frictionless disks even suggest that the stress-strain relation might not converge to a well-defined curve for larger and larger systems [32].

A rather striking feature of granular systems is the presence of force chains. These chains support most of the weight of the grains, and their geometrical characteristics —length, orientation— is the signature of the history of the system. In a recent paper [33], some of us with others have shown that it is possible to get pseudo-elastic equations from a simple model of —perfectly rigid— force chains which can split or merge at some “defects” of the grain packing. In this model, however, the stress tensor *as well as* the vector field which plays the role of the displacement in elasticity can be both built from the angular distribution of force chains. The specification of the boundary conditions is therefore a non-trivial issue on which we are currently working. There are two main advantages in this new approach. First, no real displacement field is needed, and second, it allows to calculate the pseudo-elastic coefficients from microscopic quantities —the force chains angular distribution. The idea is then to introduce some anisotropy in this distribution, and see which kind of anisotropic pseudo-elastic equations we get out of it —note that this work would be very close in spirit to, *e.g.*, [34,35] where they try to link local geometrical variables (orientation of contacts between grains) with the mechanical properties at larger scales. The fit of our data would then give information on the local structure of the packing. More response function experiments are thus planned to be performed with new preparation history, in particular with shearing or avalanching procedures in order to be able to come back to the yet unresolved sandpile “dip” problem.

It is a pleasure to thank R.P. Behringer, J.-P. Bouchaud, M.E. Cates, J. Geng, M. Otto, Y. Roichman, J.-N. Roux, D.G. Schaeffer, J.E.S. Socolar and J.P. Wittmer for very useful discussions on the problem of the response function of a granular layer. We are grateful to G. Ovarlez who did a careful check of the elastic calculations, and to E. Flavigny for making us aware of references [28] and [30]. This work has been partially supported by an Aly Kaufman postdoctoral fellowship. We acknowledge the financial support of the grant PICS-CNRS 563. D.L. acknowledges support from U.S.-Israel Binational Science Foundation grant 1999235.

Appendix A. The two-dimensional elastic calculation

For a two-dimensional elastic layer, we have three independent stress tensor components: the pressures σ_{xx} and σ_{zz} , and the shear σ_{xz} . x is the horizontal axis, and z is the vertical one, pointed downwards. The continuity equations (2) can then be explicitly written down as follows:

$$\partial_z \sigma_{zz} + \partial_x \sigma_{xz} = \rho g, \quad (\text{A.1})$$

$$\partial_z \sigma_{xz} + \partial_x \sigma_{xx} = 0. \quad (\text{A.2})$$

Besides these two equilibrium equations, an additional and independent equation is required to solve the problem. Among equations (3), the simplest is

$$\Delta(\sigma_{zz} + \sigma_{xx}) = 0. \quad (\text{A.3})$$

It is natural in this context to introduce the new variables

$$T = \sigma_{zz} + \sigma_{xx}, \quad (\text{A.4})$$

$$\tau = \sigma_{xz}, \quad (\text{A.5})$$

$$D = \sigma_{zz} - \sigma_{xx}. \quad (\text{A.6})$$

Using equations (A.1) and (A.2), it is easy to show that these new functions satisfy

$$\Delta T = 0, \quad (\text{A.7})$$

$$\Delta \tau = -\partial_x \partial_z T, \quad (\text{A.8})$$

$$\partial_x \partial_z D = (\partial_z^2 - \partial_x^2) \tau. \quad (\text{A.9})$$

A standard mathematical base of harmonic functions is the product of trigonometric functions with exponentials. We shall keep to $x \leftrightarrow -x$ symmetrical situations such that we can look for a solution of the type

$$T = B_1 z + C_1 + \int_0^{+\infty} dq \cos(qx) [a(q)e^{qz} + b(q)e^{-qz}], \quad (\text{A.10})$$

$$\tau = \frac{1}{2} B_2 x + \int_0^{+\infty} dq \sin(qx) \left\{ [c(q)e^{qz} + d(q)e^{-qz}] + \frac{1}{2} qz [a(q)e^{qz} + b(q)e^{-qz}] \right\}, \quad (\text{A.11})$$

$$D = 2\rho g z - (B_1 + B_2)z + C_2 - \int_0^{+\infty} dq \cos(qx) \left\{ qz [a(q)e^{qz} - b(q)e^{-qz}] + 2[c(q)e^{qz} - d(q)e^{-qz}] \right\}, \quad (\text{A.12})$$

where the constants B_1 , B_2 , C_1 and C_2 , as well as the functions $a(q)$, $b(q)$, $c(q)$ and $d(q)$ are to be determined by the boundary conditions.

Boundary conditions

We suppose that the top surface is submitted to a localized vertical and unitary overload, for example a normalized

Gaussian profile $Q(x)$ for the vertical pressure:

$$Q(x) = \frac{1}{\sqrt{2\pi\sigma^2}} e^{-x^2/2\sigma^2}, \quad (\text{A.13})$$

σ is the adjustable width of this overload. The two conditions at the top are then i) $\sigma_{zz}(x, 0) = Q(x)$ and ii) $\sigma_{xz}(x, 0) = 0$. Concerning the bottom, we assume that it is perfectly rigid, such that iii) $u_z(x, h) = 0$, and either very smooth or very rough. The last boundary condition is then iv-a) $\sigma_{xz}(x, h) = 0$ or iv-b) $u_x(x, h) = 0$, respectively.

It is convenient for our calculation to transform the displacement conditions iii) and iv-b) into stress conditions. For that purpose, one can take derivatives of condition iii) with respect to x and introduce stress components via the strain-stress relations. Using also equilibrium equations (A.1) and (A.2), one finally gets the condition iii):

$$(2 + \nu)\partial_x \sigma_{xz}(x, h) = \partial_z \sigma_{xx}(x, h) - \nu \rho g. \quad (\text{A.14})$$

A similar calculation leads to the following new condition iv-b):

$$\sigma_{xx}(x, h) = \nu \sigma_{zz}(x, h). \quad (\text{A.15})$$

Since we look for a solution of the form of (A.10), (A.11) and (A.12), it is natural to introduce the function $s(q)$ such that

$$Q(x) = \int_0^{+\infty} dq \cos(qx) s(q), \quad (\text{A.16})$$

which, for the specific Gaussian choice (A.13) leads to

$$s(q) = \frac{1}{\pi} e^{-\sigma^2 q^2/2}. \quad (\text{A.17})$$

Solution for a smooth bottom

We switch gravity off since it is not of interest for the calculation of the response function. A simple term-to-term identification in boundary conditions i), ii), iii) and iv-a) leads to vanishing coefficients B_i and C_i , and to the four following linear equations for the unknown functions $a(q)$, $b(q)$, $c(q)$ and $d(q)$:

$$\frac{1}{2}[a(q) + b(q)] - c(q) + d(q) = s(q), \quad (\text{A.18})$$

$$c(q) + d(q) = 0, \quad (\text{A.19})$$

$$(1 + \nu) \left\{ \left[c(q) + \frac{1}{2}qh a(q) \right] e^{qh} + \left[d(q) + \frac{1}{2}qh b(q) \right] e^{-qh} \right\} = a(q)e^{qh} - b(q)e^{-qh}, \quad (\text{A.20})$$

$$\left[c(q) + \frac{1}{2}qh a(q) \right] e^{qh} \left[d(q) + \frac{1}{2}qh b(q) \right] e^{-qh} = 0, \quad (\text{A.21})$$

whose solution is

$$a(q) = 2s(q) \frac{\sinh(qh)e^{-qh}}{\sinh(2qh) + 2qh}, \quad (\text{A.22})$$

$$b(q) = 2s(q) \frac{\sinh(qh)e^{qh}}{\sinh(2qh) + 2qh}, \quad (\text{A.23})$$

$$c(q) = -d(q) = -\frac{1}{2} s(q) \frac{2qh}{\sinh(2qh) + 2qh}. \quad (\text{A.24})$$

Putting these relations back to equations (A.10), (A.11) and (A.12), we get explicit —integral— expressions for the stress components. Note that the function a , b , c and d are independent of ν .

Solution for a rough bottom

For the case of a rough bottom, condition iv-a) has to be replaced by condition iv-b). It means that the last equation of the system (A.18-A.21) has to be changed into

$$-\left[c(q) + \frac{1}{2}qh a(q)\right] e^{qh} + \left[d(q) + \frac{1}{2}qh b(q)\right] e^{-qh} = \frac{1}{2} \frac{1-\nu}{1+\nu} [a(q)e^{qh} + b(q)e^{-qh}] \quad (\text{A.25})$$

and the resolution of these four linear equations leads this time to the following solution:

$$a(q) = 2s(q) \frac{f_-(q) + 2qh}{f_+(q)f_-(q) + 4q^2h^2}, \quad (\text{A.26})$$

$$b(q) = 2s(q) \frac{f_+(q) - 2qh}{f_+(q)f_-(q) + 4q^2h^2}, \quad (\text{A.27})$$

$$c(q) = -d(q) = -\frac{1}{2} s(q) \left[1 - \frac{f_+(q) + f_-(q)}{f_+(q)f_-(q) + 4q^2h^2}\right], \quad (\text{A.28})$$

where the functions f_+ and f_- are defined by

$$f_{\pm}(q) = 1 + \frac{3-\nu}{1+\nu} e^{\pm 2qh}. \quad (\text{A.29})$$

This time, there is a dependence on ν . In principle, the Poisson coefficient should be less than unity in $2d$. However, these functions really change behaviour only for $\nu \geq 3$, leading to oscillatory stresses —they however develop negative parts as $\nu \rightarrow 3$.

Semi-infinite medium

For comparison, in the case of a semi-infinite medium submitted to a vertical unitary force localized at $x = 0$, the stress components are given [13] by

$$\sigma_{zz} = \frac{2}{\pi} \frac{z^3}{(x^2 + z^2)^2}, \quad (\text{A.30})$$

$$\sigma_{xx} = \frac{2}{\pi} \frac{zx^2}{(x^2 + z^2)^2}, \quad (\text{A.31})$$

$$\sigma_{xz} = \frac{2}{\pi} \frac{xz^2}{(x^2 + z^2)^2}. \quad (\text{A.32})$$

Appendix B. The three-dimensional case

The calculation in the three-dimensional case is very similar to the $2d$ one. We shall keep to axi-symmetric situations so that the stress tensor has only four non-zero components: the pressures σ_{zz} , σ_{rr} , $\sigma_{\theta\theta}$ and the shear σ_{rz} . z

is again the vertical axis pointing downwards, and (r, θ) are the horizontal planar coordinates.

The equations we want to solve are simpler with the new functions

$$T = \sigma_{zz} + \sigma_{rr} + \sigma_{\theta\theta}, \quad (\text{B.1})$$

$$\tau = \sigma_{rz}, \quad (\text{B.2})$$

$$S = \sigma_{rr} + \sigma_{\theta\theta}, \quad (\text{B.3})$$

$$D = \sigma_{rr} - \sigma_{\theta\theta}, \quad (\text{B.4})$$

which must satisfy

$$\Delta T = 0, \quad (\text{B.5})$$

$$(1 + \nu)\Delta S = \partial_z^2 T, \quad (\text{B.6})$$

$$\partial_r \tau + \frac{\tau}{r} = -\partial_z(T - S) + \rho g, \quad (\text{B.7})$$

$$\partial_r D + 2\frac{D}{r} = -\partial_r S - 2\partial_z \tau. \quad (\text{B.8})$$

The last two equations are the explicit forms of the force balance equations (2), and we got the two first ones from equations (3).

The corresponding general solutions involve Bessel functions of the first kind J_0 , J_1 and J_2 , and read:

$$T = T_1 z + T_2 + \int_0^{+\infty} dq J_0(qr) [a(q)e^{qz} + b(q)e^{-qz}], \quad (\text{B.9})$$

$$S = S_1 z + S_2 + \int_0^{+\infty} dq J_0(qr) \left\{ [c(q)e^{qz} + d(q)e^{-qz}] + \frac{1}{2} \frac{1}{1+\nu} qz [a(q)e^{qz} - b(q)e^{-qz}] \right\}, \quad (\text{B.10})$$

$$\tau = \frac{1}{2} \rho g r + \frac{1}{2} r(S_1 - T_1) + \frac{u(z)}{r} + \int_0^{+\infty} dq J_1(qr) \left\{ [c(q) - a(q)]e^{qz} + [d(q) - b(q)]e^{-qz} \right\} + \frac{1}{2} \frac{1}{1+\nu} \int_0^{+\infty} dq J_1(qr) \left\{ a(q)[1 + qz]e^{qz} - b(q)[1 - qz]e^{-qz} \right\}, \quad (\text{B.11})$$

$$D = \frac{v(z)}{r^2} - \frac{du(z)}{dz} + \int_0^{+\infty} dq J_2(qr) \left\{ [2a(q) - c(q)]e^{qz} + [2b(q) - d(q)]e^{-qz} \right\} - \frac{1}{1+\nu} \int_0^{+\infty} dq J_2(qr) \times \left\{ a(q) \left[2 + \frac{1}{2} qz \right] e^{qz} + b(q) \left[2 - \frac{1}{2} qz \right] e^{-qz} \right\}, \quad (\text{B.12})$$

where the constants T_1 , T_2 , S_1 and S_2 , as well as the functions $u(z)$, $v(z)$, $a(q)$, $b(q)$, $c(q)$ and $d(q)$ are, again, to be determined by the boundary conditions.

Boundary conditions

As in the $2d$ case, we want to impose at the surface i) an overload $\sigma_{zz}(r, 0) = Q(r)$, but ii) no shear $\sigma_{rz}(r, 0) = 0$. At the bottom, the vertical displacement must vanish $u_z(r, h) = 0$ iii), and we shall study the two cases, very smooth $\sigma_{rz}(r, h) = 0$ iv-a) or very rough $u_r(r, h) = 0$ iv-b) bottom.

The $3d$ equivalent of (A.13) is now

$$Q(r) = \frac{1}{2\pi\sigma^2} e^{-r^2/2\sigma^2}. \quad (\text{B.13})$$

Looking at the general form of the solution (B.9-B.12), it is natural to introduce the function $s(q)$ defined by the relation

$$Q(r) = \int_0^{+\infty} dq J_0(qr) s(q), \quad (\text{B.14})$$

which, for Q given by (B.13), gives

$$s(q) = \frac{1}{2\pi} q e^{-\sigma^2 q^2/2}. \quad (\text{B.15})$$

Taking derivatives of the conditions on displacements and using stress-strain relations, one can again transform these conditions into relations between stress components only. It is easy to show that condition iii) can be written as

$$2(1 + \nu)\partial_r \tau = \frac{1}{2}(1 + \nu)\partial_z(S + D) - \nu\partial_z T, \quad (\text{B.16})$$

and that condition iv-b) gives

$$(1 + \nu)(S + D) = 2\nu T \quad (\text{B.17})$$

(these last two relations are only valid at $z = h$).

Solution for a smooth bottom

Again, as we are interested in the response of the elastic layer to this overload, gravity is switched off. The four conditions i)-iv-a) then give four equations for the unknown functions $a(q)$, $b(q)$, $c(q)$ and $d(q)$, all other functions and constants being zero. These equations are

$$a(q) + b(q) - c(q) - d(q) = s(q), \quad (\text{B.18})$$

$$c(q) - d(q) = \frac{1 + 2\nu}{2(1 + \nu)} [a(q) - b(q)], \quad (\text{B.19})$$

$$2(1 + \nu) [c(q)e^{qh} - d(q)e^{-qh}] = (3 - qh)a(q)e^{qh} - (3 + qh)b(q)e^{-qh}, \quad (\text{B.20})$$

$$2(1 + \nu) [c(q)e^{qh} - d(q)e^{-qh}] = (1 + 2\nu - qh)a(q)e^{qh} - (1 + 2\nu + qh)b(q)e^{-qh}, \quad (\text{B.21})$$

whose solution is

$$a(q) = 2s(q)(1 + \nu) \frac{\sinh(qh)e^{-qh}}{\sinh(2qh) + 2qh}, \quad (\text{B.22})$$

$$b(q) = 2s(q)(1 + \nu) \frac{\sinh(qh)e^{qh}}{\sinh(2qh) + 2qh}, \quad (\text{B.23})$$

$$c(q) = -\frac{1}{2}s(q) \times \left[1 - (3 + 4\nu) \frac{\sinh(qh)e^{-qh}}{\sinh(2qh) + 2qh} - \frac{\sinh(qh)e^{qh}}{\sinh(2qh) + 2qh} \right], \quad (\text{B.24})$$

$$d(q) = -\frac{1}{2}s(q) \times \left[1 - \frac{\sinh(qh)e^{-qh}}{\sinh(2qh) + 2qh} - (3 + 4\nu) \frac{\sinh(qh)e^{qh}}{\sinh(2qh) + 2qh} \right]. \quad (\text{B.25})$$

Solution for a rough bottom

In the case of a very rough bottom, the relation (B.21) should be replaced by the condition iv-b), *i.e.* by

$$2(1 + \nu) [c(q)e^{qh} + d(q)e^{-qh}] = (4\nu - qh)a(q)e^{qh} + (4\nu + qh)b(q)e^{-qh}. \quad (\text{B.26})$$

The resolution of the four equations then gives

$$a(q) = 2s(q)(1 + \nu) \frac{f_-(q) + 2qh}{f_+(q)f_-(q) + 4q^2h^2}, \quad (\text{B.27})$$

$$b(q) = 2s(q)(1 + \nu) \frac{f_+(q) - 2qh}{f_+(q)f_-(q) + 4q^2h^2}, \quad (\text{B.28})$$

$$c(q) = -\frac{1}{2}s(q) \times \left[1 - \frac{(3 + 4\nu)f_-(q) + f_+(q) + 4qh(1 + 2\nu)}{f_+(q)f_-(q) + 4q^2h^2} \right], \quad (\text{B.29})$$

$$d(q) = -\frac{1}{2}s(q) \times \left[1 - \frac{(3 + 4\nu)f_+(q) + f_-(q) - 4qh(1 + 2\nu)}{f_+(q)f_-(q) + 4q^2h^2} \right], \quad (\text{B.30})$$

where the functions f_+ and f_- are defined by

$$f_{\pm}(q) = 1 + (3 - 4\nu) e^{\pm 2qh}. \quad (\text{B.31})$$

Again, as in the $2d$ case, the usual bound $\nu = \frac{1}{2}$ can be exceeded without quantitative change—except the appearance of negative parts—up to $\nu = \frac{3}{4}$, where the stresses start oscillating.

Semi-infinite medium

For comparison, in the case of a semi-infinite medium submitted to a vertical unitary force localized at $r = 0$, the stress components are given by Boussinesq and Cerruti's

formulae [27]:

$$\sigma_{zz} = \frac{3}{2\pi} \frac{z^3}{(r^2 + z^2)^{5/2}}, \quad (\text{B.32})$$

$$\sigma_{rr} = \frac{1}{2\pi} \left[(1 - 2\nu) \times \left(\frac{1}{r^2} - \frac{z}{r^2(r^2 + z^2)^{1/2}} \right) - \frac{3zr^2}{(r^2 + z^2)^{5/2}} \right], \quad (\text{B.33})$$

$$\sigma_{\theta\theta} = \frac{1}{2\pi} (1 - 2\nu) \times \left(\frac{1}{r^2} - \frac{z}{r^2(r^2 + z^2)^{1/2}} - \frac{z}{(r^2 + z^2)^{3/2}} \right), \quad (\text{B.34})$$

$$\sigma_{rz} = \frac{3}{2\pi} \frac{rz^2}{(r^2 + z^2)^{5/2}}. \quad (\text{B.35})$$

References

1. P.-G. de Gennes, *Rev. Mod. Phys.* **71**, S374 (1999).
2. D.M. Wood, *Soil Behaviour and Critical State Soil Mechanics* (Cambridge University Press, Cambridge, 1990).
3. X. Jia, C. Caroli, B. Velicky, *Phys. Rev. Lett.* **82**, 1863 (1999).
4. F. Radjai, D.E. Wolf, M. Jean, J.-J. Moreau, *Phys. Rev. Lett.* **80**, 61 (1998).
5. C.-h. Liu, S.R. Nagel, *Phys. Rev. Lett.* **68**, 2301 (1992); *Phys. Rev. B* **48**, 15646 (1993).
6. J. Šmíd, J. Novosad, *Proc. Powtech. Conference 1981*, Ind. Chem. Eng. Symp. **63**, D3V 1 (1981); R. Brockbank, J.M. Huntley, R.C. Ball, *J. Phys. II* **7**, 1521 (1997).
7. L. Vanel, D.W. Howell, D. Clark, R.P. Behringer, E. Clément, *Phys. Rev. E* **60**, R5040 (1999).
8. J.-P. Bouchaud, M.E. Cates, P. Claudin, *J. Phys. I* **5**, 639 (1995).
9. J.P. Wittmer, P. Claudin, M.E. Cates, J.-P. Bouchaud, *Nature* **382**, 336 (1996); J.P. Wittmer, P. Claudin, M.E. Cates, *J. Phys. I* **7**, 39 (1997).
10. L. Vanel, P. Claudin, J.-P. Bouchaud, M.E. Cates, E. Clément, J.P. Wittmer, *Phys. Rev. Lett.* **84**, 1439 (2000).
11. S.B. Savage, in *Physics of Dry Granular Media*, edited by H.J. Herrmann, J.P. Hovi, S. Luding, *NATO ASI Ser.*, Vol. **25** (Kluwer, Amsterdam, 1997).
12. P. Dantu, *Ann. Ponts Chaussées* **4**, 144 (1967); G. Josselin de Jong, A. Verruijt, *Cah. Groupe Fr. Rheol.* **2**, 73 (1969).
13. L. Landau, E. Lifshitz, *Elasticity Theory* (Pergamon Press, New York, 1986).
14. G. Reydellet, E. Clément, *Phys. Rev. Lett.* **86**, 3308 (2001).
15. J. Geng, D. Howell, E. Longhi, R.P. Behringer, G. Reydellet, L. Vanel, E. Clément, S. Luding, *Phys. Rev. Lett.* **87**, 035506 (2001).
16. N. Mueggenburg, H. Jaeger, S. Nagel, private communication.
17. C. Eloy, E. Clément, *J. Phys. I* **7**, 1541 (1997).
18. J.-J. Moreau, in the Proceedings of the *Colloque "Physique et mécanique des matériaux granulaires"*, Champs-sur-Marne (France), Vol. **199** (LCPC, 2000).
19. S.F. Edwards, *Physica A* **249**, 226 (1998); S.F. Edwards, D.V. Grinev, *Phys. Rev. Lett.* **82**, 5397 (1999).
20. A.V. Tkachenko, T.A. Witten, *Phys. Rev. E* **60**, 687 (1999); **62**, 2510 (2000).
21. J.-N. Roux, *Phys. Rev. E* **61**, 6802 (2000).
22. C.F. Moukarzel, *Phys. Rev. Lett.* **81**, 1634 (1998).
23. D.A. Head, A.V. Tkachenko, T.A. Witten, *Eur. Phys. J. E* **6**, 99 (2001).
24. M. da Silva, J. Rajchenbach, *Nature* **406**, 70 (2000).
25. C.-h. Liu, S.R. Nagel, D.A. Schecter, S.N. Coppersmith, S. Majumdar, O. Narayan, T.A. Witten, *Science* **269**, 513 (1995); S.N. Coppersmith, C.-h. Liu, S. Majumdar, O. Narayan, T.A. Witten, *Phys. Rev. E* **53**, 4673 (1996).
26. P. Evesque, P.-G. de Gennes, *C. R. Acad. Sci. (Paris)* **326**, Sér. II, 761 (1998).
27. K.L. Johnson, *Contact Mechanics* (Cambridge University Press, Cambridge, 1985).
28. J.-P. Giroud, *Tables pour le calcul des fondations* (Dunod, Paris, 1972).
29. N.I. Muskhelishvili, *Some Basic Problems of the Mathematical Theory of Elasticity* (P. Noordhoff Ltd, Groningen, 1963).
30. J. Garnier, *Tassement et contraintes. Influence de la rigidité de la fondation et de l'anisotropie du massif*, PhD thesis, Université de Grenoble (1973).
31. B. Cambou, M. Chaze, F. Dedecker, *Eur. J. Mech. A/Solids* **19**, 999 (2000).
32. G. Combe, J.-N. Roux, *Phys. Rev. Lett.* **85**, 3628 (2000).
33. J.-P. Bouchaud, P. Claudin, D. Levine, M. Otto, *Eur. Phys. J. E* **4**, 451 (2001).
34. F. Calvetti, G. Combe, J. Lanier, *Mech. Coh. Frict. Mater.* **2**, 121 (1997).
35. F. Radjai, S. Roux, *Powders and Grains 2001*, edited by Y. Kishino, (Balkema, Lisse, 2001) p. 21.